

Neutron capture measurements for s-process nucleosynthesis

A review about CERN n_TOF developments and contributions

C. Domingo-Pardo¹, O. Aberle², V. Alcayne³, G. Alpar⁴, M. Al Halabi⁵, S. Amaducci⁶, V. Babiano⁷, M. Bacak^{2,8}, J. Balibrea-Correa¹, J. Bartolomé⁹, A. P. Bernardes², B. Bernardino Gameiro¹, E. Berthoumieux¹⁰, R. Beyer¹¹, M. Birch⁸, M. Boromiza¹², D. Bosnar¹³, B. Brusasco⁷, M. Caamaño¹⁴, A. Cahuzac¹⁰, F. Calviño⁷, M. Calviani², D. Cano-Ott³, A. Casanovas⁷, D. M. Castelluccio^{15,16}, D. Catlett⁴, F. Cerutti², G. Cescutti^{17,18}, E. Chiaveri^{2,8}, G. Claps¹⁹, P. Colombetti^{20,21}, N. Colonna²², P. Console Camprini^{15,16}, G. Cortés⁷, M. A. Cortés-Giraldo⁹, L. Cosentino⁶, S. Cristallo^{23,24}, A. D'Ottavi⁸, G. de la Fuente Rosales¹, S. F. Dellmann⁵, M. Diakaki²⁵, M. Di Castro², A. Di Chicco²⁶, M. Dietz²⁶, E. Dupont¹⁰, I. Durán¹⁴, Z. Eleme²⁷, M. Eslami²⁸, S. Fargier², B. Fernández-Domínguez¹⁴, P. Finocchiaro⁶, W. Flanagan⁴, V. Furman²⁹, A. Gandhi¹², F. García-Infantes^{30,2}, A. Gawlik-Ramiega³¹, G. Gervino^{20,21}, S. Gilardoni², E. González-Romero³, S. Goula²⁷, E. Griesmayer³², C. Guerrero⁹, F. Gunsing¹⁰, C. Gustavino³³, J. Heyse³⁴, W. Hillman⁸, D. G. Jenkins²⁸, E. Jericha³², A. Junghans¹¹, Y. Kadi², K. Kaperoni²⁵, I. Kelly⁴, M. Kokkoris²⁵, Y. Kopatch²⁹, M. Krčička³⁵, N. Kyritsis²⁵, C. Lederer-Woods³⁶, J. Lerendegui-Marco¹, A. Manna^{16,37}, T. Martínez³, M. Martínez-Cañada³⁰, A. Masi², C. Massimi^{16,37}, P. Mastinu³⁸, M. Mastromarco^{22,39}, E. A. Mauger⁴⁰, A. Mazzone^{22,41}, E. Mendoza³, A. Mengoni^{15,16}, V. Michalopoulou²⁵, P. M. Milazzo¹⁷, J. Moldenhauer⁴, R. Mucciola²², E. Musacchio González³⁸, A. Musumarra^{42,43}, A. Negret¹², E. Odusina³⁶, D. Papanikolaou⁴², N. Patronis^{27,2}, J. A. Pavón-Rodríguez⁹, M. G. Pellegriti⁴², P. Pérez-Maroto⁹, A. Pérez de Rada Fiol³, G. Peretto²², J. Perkowski³¹, C. Petrone¹², N. Pieretti^{16,37}, L. Piersanti^{23,24}, E. Pirovano²⁶, I. Porras³⁰, J. Praena³⁰, J. M. Quesada⁹, R. Reifarh⁵, D. Rochman⁴⁰, Y. Romanets⁴⁴, A. Rooney³⁶, G. Rovira⁴⁵, C. Rubbia², A. Sánchez-Caballero³, R. N. Sahoo¹⁶, D. Scarpa³⁸, P. Schillebeeckx³⁴, A. G. Smith⁸, N. V. Sosnin^{36,8}, M. Spelta^{17,18}, M. E. Stamati^{27,2}, K. Stasiak³¹, G. Tagliente²², A. Tarifeño-Saldivia¹, D. Tarrío⁴⁶, P. Torres-Sánchez¹, S. Tosi¹⁹, G. Tsileadakis¹⁰, S. Valenta³⁵, P. Vaz⁴⁴, G. Vecchio⁶, D. Vescovi^{23,24}, V. Vlachoudis², R. Vlastou²⁵, A. Wallner¹¹, C. Weiss³², P. J. Woods³⁶, T. Wright⁸, R. Wu²⁸, P. Žugec¹³, The n_TOF Collaboration (www.cern.ch/ntof)

¹Instituto de Física Corpuscular, CSIC - Universidad de Valencia, Spain ²European Organization for Nuclear Research (CERN), Switzerland ³Centro de Investigaciones Energéticas Medioambientales y Tecnológicas (CIEMAT), Spain ⁴University of Dallas, USA ⁵Goethe University Frankfurt, Germany ⁶INFN Laboratori Nazionali del Sud, Catania, Italy ⁷Universitat Politècnica de Catalunya, Spain ⁸University of Manchester, United Kingdom ⁹Universidad de Sevilla, Spain ¹⁰CEA Irfu, Université Paris-Saclay, F-91191 Gif-sur-Yvette, France ¹¹Helmholtz-Zentrum Dresden-Rossendorf, Germany ¹²Horia Hulubei National Institute of Physics and Nuclear Engineering, Romania ¹³Department of Physics, Faculty of Science, University of Zagreb, Zagreb, Croatia ¹⁴University of Santiago de Compostela, Spain ¹⁵Agenzia nazionale per le nuove tecnologie, l'energia e lo sviluppo economico sostenibile (ENEA), Italy ¹⁶Istituto Nazionale di Fisica Nucleare, Sezione di Bologna, Italy ¹⁷Istituto Nazionale di Fisica Nucleare, Sezione di Trieste, Italy ¹⁸Department of Physics, University of Trieste, Italy ¹⁹INFN Laboratori Nazionali di Frascati, Italy ²⁰Istituto Nazionale di Fisica Nucleare, Sezione di Torino, Italy ²¹Department of Physics, University of Torino, Italy ²²Istituto Nazionale di Fisica Nucleare, Sezione di Bari, Italy ²³Istituto Nazionale di Fisica Nucleare, Sezione di Perugia, Italy ²⁴Istituto Nazionale di Astrofisica - Osservatorio Astronomico d'Abruzzo, Italy ²⁵National Technical University of Athens, Greece ²⁶Physikalisch-Technische Bundesanstalt (PTB), Bundesallee 100, 38116 Braunschweig, Germany ²⁷University of Ioannina, Greece ²⁸University of York, United Kingdom ²⁹Affiliated with an institute covered by a cooperation agreement with CERN ³⁰University of Granada, Spain ³¹University of Lodz, Poland ³²TU Wien, Atominstytut, Stadionallee 2, 1020 Wien, Austria ³³Istituto Nazionale di Fisica Nucleare, Sezione di Roma1, Roma, Italy ³⁴European Commission, Joint Research Centre (JRC), Geel, Belgium ³⁵Charles University, Prague, Czech Republic ³⁶School of Physics and Astronomy, University of Edinburgh, United Kingdom ³⁷Dipartimento di Fisica e Astronomia, Università di Bologna, Italy ³⁸INFN Laboratori Nazionali di Legnaro, Italy ³⁹Dipartimento Interateneo di Fisica, Università degli Studi di Bari, Italy ⁴⁰Paul Scherrer Institut (PSI), Villigen, Switzerland ⁴¹Consiglio Nazionale delle Ricerche, Bari, Italy ⁴²Istituto Nazionale di Fisica Nucleare, Sezione di Catania, Italy ⁴³Department of Physics and Astronomy, University of Catania, Italy ⁴⁴Instituto Superior Técnico, Lisbon, Portugal ⁴⁵Japan Atomic Energy Agency (JAEA), Tokai-Mura, Japan ⁴⁶Department of Physics and Astronomy, Uppsala University, Box 516, 75120 Uppsala, Sweden

Received: February 17, 2025/ Revised version: February 17, 2025

Abstract. This article presents a review about the main CERN n_TOF contributions to the field of neutron-capture experiments of interest for s-process nucleosynthesis studies over the last 25 years, with special focus on the measurement of radioactive isotopes. A few recent capture experiments on stable isotopes of astrophysical interest are also discussed. Results on s-process branching nuclei are appropriate to illustrate how advances in detection systems and upgrades in the facility have enabled increasingly challenging experiments and, as a consequence, have led to a better understanding and modeling of the s-process mechanism of nucleosynthesis. New endeavors combining radioactive-ion beams from ISOLDE for the production of radioisotopically pure samples for activation experiments at the new NEAR facility at n_TOF are briefly discussed. On the basis of these new exciting results, also current limitations of state-of-the-art TOF and activation techniques will be depicted, thereby showing the pressing need for further upgrades and enhancements on both facilities and detection systems. A brief account of the potential technique based on inverse kinematics for direct neutron-capture measurements is also presented.

1 Introduction

Neutron-capture reactions play a fundamental role in the cosmic origin of elements heavier than iron, both during hydrostatic stages of stellar evolution (*s*-process) and in cataclysmic stellar environments (*r*-process). These two nucleosynthesis mechanisms were first presented in detail in the works of B2FH [1] and Cameron [2]. As a consequence, a large experimental effort over the last 70 years has resulted in a wealth of neutron-capture nuclear data. The first experiments were initially aimed at validating the *s*-process hypothesis [3,4], and shortly afterwards to aid in the development and refinement of stellar models while constraining the physical conditions along different evolutionary stages of stars [5,6]. See also the review of Käppeler et al. [7] and references therein.

Two different methodologies for neutron-capture cross section measurements have been extensively applied so far in many laboratories worldwide, neutron time-of-flight (TOF) and neutron activation, thereby covering about 350 (predominantly stable) nuclei [8]. However, there are still acute needs for new neutron-capture cross-section measurements and for a large fraction of the measured isotopes improvements are required both in terms of accuracy and energy-range completeness.

From the astrophysical standpoint there are three “families” of nuclides with a particular value for *s*-process studies. The group of *s*-only nuclei serves as a benchmark for *s*-process and galactic-chemical evolution (GCE) models, which should reproduce 100% of the *s*-only isotopic abundances [9,10,11]. The group of *s*-process bottlenecks gives rise to the three characteristic *s*-process abundance peaks at the neutron-shell closures $N = 50, 82$ and 126 . Because of their large abundances, elements in the bottleneck peaks show-up prominently in spectroscopic observations of stellar atmospheres and thus, they represent a sensible probe for stellar models. Finally, *s*-process branching nuclei are especially relevant for constraining the physical conditions of the stellar environment [7]. Interestingly, for none of these groups the quality of the data complies with the $\pm 5\%$ uncertainty level required by stellar models. The neutron-capture cross sections of most *s*-only nuclei are relatively well determined [8], which does not necessarily imply that their *s*-process abundances are correspondingly accurate. This is a consequence of the strong interplay between many *s*-process branchings and *s*-only isotopes [12,10]. The astrophysical impact of the uncertainties on the *s*-process branchings is therefore twofold, because the final *s*-only abundances are important both for benchmarking the performance of stellar models [13] and for deriving the isotopic *r*-process abundance distributions in the solar system [14,15,11].

Past and ongoing efforts at CERN n_TOF to improve this situation are described in this article. A large number of articles describe already the n_TOF facility and the related measuring technics in great detail [16,17,18,19,20] and thus, only some main facility features relevant for the discussions in the present article will be summarized

in Sec.2. Because of their relevance for *s*-process nucleosynthesis and the demanding features of the experiments, measurements on unstable *s*-process branching nuclei are well suited to illustrate the experimental progress achieved over the last 25 years. Thus, Sec.3 presents in chronological order the main results on *s*-process branching nuclei measured at n_TOF, along with the facility and detector advances that were relevant for such studies. Measurements on stable isotopes involved in the *s*-process path are also of paramount importance for properly interpreting observed elemental abundances in stars and isotopic analysis of meteorites, and thus for a better understanding of the *s*-process mechanism. Some recent examples will be discussed in Sec.4. Finally, Sec.5 summarizes some of the main limitations of state-of-the-art TOF experiments, and presents ongoing efforts to improve present instruments and to complement them with new measuring stations and techniques.

2 The n_TOF facility

n_TOF utilizes a 6 ns wide, 20 GeV pulsed proton beam from CERN’s Proton Synchrotron (PS), typically delivering nowadays 8×10^{12} protons per pulse to a lead spallation target (Fig.1), where approximately 300 neutrons are produced per incident proton. The neutron energy is determined with a high precision by means of the time-of-flight technique [21]. The low duty cycle and the high instantaneous flux are two of the most remarkable facility features. Neutron bunches are spaced at intervals of at least 1.2 seconds, corresponding to the operational cycle of the CERN Proton Synchrotron (PS). This duty cycle enables measurements over an extended TOF span, facilitating the detection of low-energy neutrons without overlap from subsequent neutron cycles. As a result, neutron energies as low as approximately 10 meV can be measured, with the high-energy portion of the spectrum remaining unaffected by slow neutrons from previous cycles. On the other hand, the exceptionally high instantaneous neutron flux is particularly advantageous when working with radioactive samples, as it ensures a highly favorable ratio of neutron-induced reaction signals to background signals caused by radioactive decay events.

At the core of the facility, the optimization of the spallation target has been one of the key aspects for the successful realization of neutron-capture experiments (see Fig. 1). A layer of water moderates the initially fast neutrons into a white spectrum covering a broad energy range from meV to GeV, thus fully including the energy-range of astrophysical interest for *s*-process studies (~ 1 eV - 100 keV). During phase-I (2001-2004) a water layer served as coolant and moderator for a $80 \times 80 \times 60$ cm³ lead target (Fig.1). This design severely limited the lifetime of the target owing to corrosion effects and, more relevant for capture experiments, contaminant neutron-capture reactions in the hydrogen of the water induced a large in-beam γ -ray background. The latter was a minor issue for the measurement of isotopes with large capture cross sections, like unstable ¹⁵¹Sm [24], but it made quite difficult the measure-



Fig. 1. From left to right, the three generations of spallation sources at n_TOF. The latest version [22] delivers a superior neutron-beam quality for capture experiments at both measuring stations EAR1 (185 m) and EAR2 (20 m) [23].

ment of neutron-magic isotopes with small capture cross sections, like ^{208}Pb or ^{209}Bi [25]. A new cylindrical (40 cm length, 60 cm diameter) target design (see Fig.1) incorporated several improvements for phase-II (2009-2012), among them the use of a 1 cm water cooling circuit and a separate ^{10}B -loaded 4-cm thick demineralized-water moderator, which efficiently suppressed the in-beam ($E_\gamma=2.2$ MeV) γ -ray background. However, during the last years of operation an increase in the activity of the cooling circuit was detected, which was ascribed to corrosion in the lead-water interface. In 2014 a second experimental area EAR2 was constructed at only 20 m above the already existing spallation target [26,27]. The new measuring extension allowed one to significantly extend the number of experiments during phase-III (2014-2018) (see Fig.1 in Ref.[20]). Initially, the large instantaneous flux of EAR2 could not be efficiently exploited for *s*-process capture studies due to the fact that the target geometry and moderator characteristics were not optimal for the new EAR2 station [28, 29]. However, all these limitations were remarkably improved in phase-IV (2021-) with the third-generation neutron target [22] (see Fig.1). With the new target a slightly higher neutron flux was achieved and, more importantly, the resolution function (RF) at EAR2 could be significantly enhanced (see Fig.2 in [23]). A large instantaneous neutron flux and a narrow resolution-function become of special importance for astrophysics experiments [30] and thus, the new target features enabled at EAR2 some of the most challenging and fascinating neutron-capture TOF experiments performed so far, as it is discussed below.

3 Progress on *s*-process branching isotopes

Unstable nuclei with relatively long half-lives ($\sim\text{yr}$) are particularly interesting for *s*-process studies because they produce a split in the *s*-process path. The strength of the branching determines the local isotopic pattern around the unstable nucleus and the resulting isotopic abundances become sensitive to the physical conditions of the stellar environment [7]. Therefore, accurate neutron-capture

cross section measurements on these nuclides in combination with isotopic analysis of meteorites and state-of-the-art stellar models may provide correspondingly valuable constraints on the thermal- and neutron-density conditions of the stellar environment. From the experimental viewpoint, producing (radioactive) samples with sufficient number of atoms ($\geq 10^{18}$ atoms), and with high enough enrichment becomes a true challenge. For most of the experiments discussed in this section a sample-production strategy based on the combined effort from Institut Laue-Langevin (ILL)-Grenoble (France) and Paul Scherrer Institute (PSI)-Villigen (Switzerland) was pursued. At ILL isotope-production via thermal-neutron activation was carried out, while the radiochemistry laboratory of PSI produced the samples for irradiation at ILL and in some cases performed a posterior radiochemical separation and purification. Still, many of the measured radioactive samples posed important challenges for the capture experiment, which were mainly related to the sample radioactivity, to the final number of atoms available for the isotope of interest and to the sample purity or enrichment. In order to cope with such demanding cases, a big effort has been made over the last 25 years at CERN n_TOF for optimizing the quality of the neutron beam in terms of resolution function, high instantaneous neutron flux and low gamma- and neutron-induced backgrounds. In addition, both continuous adaptations and disruptive approaches have been pursued with the detection systems, leading to a progressive increase in detection sensitivity for the radiative neutron-capture channel of astrophysical interest. These advances are described in more detail below. Such progress can be well illustrated via the measured *s*-process branching isotopes and the corresponding facility and detector upgrades. To do so, a figure of merit (FOM) is arbitrarily defined here as

$$FOM = \frac{1}{m_i \cdot \sigma_i \cdot f_e}, \quad (1)$$

where m_i is the mass of the isotope of interest in the sample (in mg), σ_i is the Maxwellian capture cross section at 30 keV (in mb), and f_e is the enrichment factor for the

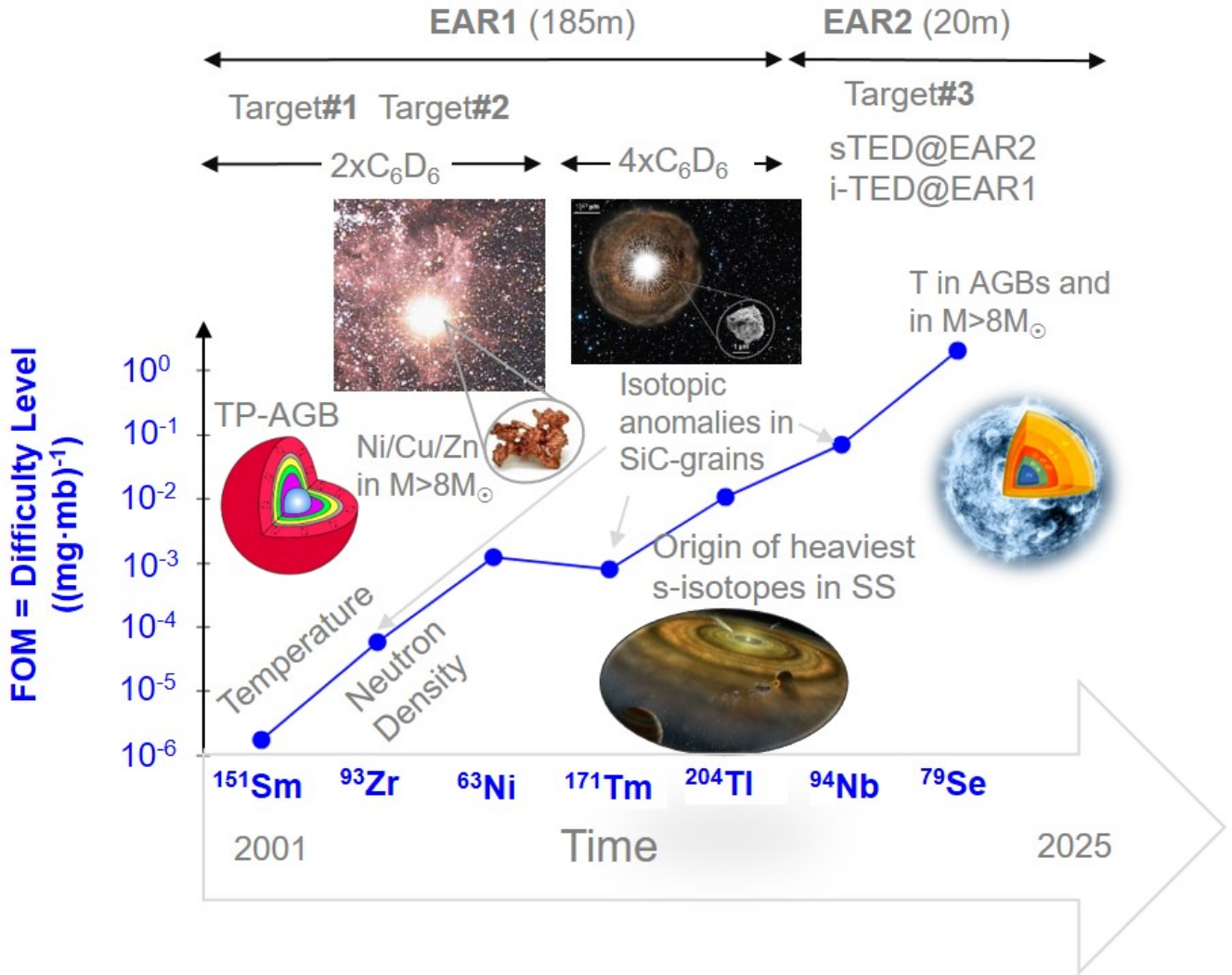


Fig. 2. Advances in facility upgrades and detection systems at CERN n_TOF have led to increasingly difficult experiments on *s*-process branching nuclei along the last two decades. See text for details on the different *s*-process branching cross-section measurements. For Target#1-3 see Fig.1 and for the detection system refer to Fig.3 and Fig.4. Credits for figure insets: TP-AGB drawing adapted from [31]; HST image of the TP-AGB U. Camelopardalis with a SiC grain (NASA/Nan Liu/Andrew Davis), massive-star illustration (NASA/CXC/M. Weiss).

isotope of interest in the sample. This FOM will be also referred to as "difficulty level" along this article, and it is shown in Fig. 2 as a function of the *s*-process branching isotope measured (published) along the different years. In short, the smaller are the sample mass, the cross section and the enrichment, the more difficult it becomes to perform the measurement. The FOM does not include the half-life of the isotope, nor the difficulty ascribed to the background induced by the sample-decay itself, which can be very different depending on whether there is emission of high-energy γ -rays or not. However, as we will see, for the cases and the range of half-lives discussed here (2 yr – 4 Myr) there is no correlation between difficulty and half-life, because the other ingredients became a much more significant constraint for the measurement. Remarkably, as it will be seen later, at least for the cases described here the main limitations in terms of sample-radioactivity

were not due to the decay of the isotope of interest itself, but rather to different levels of ^{60}Co contamination in the samples (see discussion below for ^{204}Tl , ^{94}Nb and ^{79}Se).

A more relevant ingredient, which is not included in the FOM, is the effective neutron-energy range actually covered in the measurement or the neutron-energy range, which is usable in the analysis of the capture data. This aspect is difficult to include in such a FOM and, as we will see, it is worth recognizing that an effort should be made to extend the energy range for most of the measured *s*-process branching points discussed here, once alternative approaches or improved measuring conditions become available in the future.

$^{151}\text{Sm}(n, \gamma)$: temperature in He-shell flashes of low-mass red giant stars

^{151}Sm ($t_{1/2} = 94.6$ y) was the very first *s*-process branching measured at the beginning of the n_TOF experiment in 2001 and published in 2004 [24]. A highly enriched ($\sim 90\%$) sample of ^{151}Sm with a mass of 206 mg (8×10^{20} atoms) was measured at the EAR1 station using a set of two C_6D_6 detectors placed at 90° with respect to the beam axis at the sample position (see Fig.3). These detectors were designed with the aim of enhancing detection efficiency and reducing neutron-induced backgrounds [32] (see also discussion in Sec.4). Both in-beam γ -rays background and the high sample activity (156 GBq) played a minor role over the entire energy range of interest for this measurement (see Fig.2 in [24]) due to the large capture cross section (~ 3 b at 30 keV) and the fact that ^{151}Sm decays via pure β emission without high-energy γ -rays. Despite being the very first TOF measurement of the neutron-capture cross section of ^{151}Sm it was quite straight-forward and, quite remarkably, the neutron-capture cross section could be determined over the full stellar energy range of astrophysical relevance (see Fig.2 in [24]). This feature could not be matched by any *s*-process branching nuclei measured later due to the much more difficult experimental conditions.

Although the limitations of the phenomenological *s*-process model [33] were already uncovered many years before after a series of dedicated experiments at the Karlsruhe Van de Graaff accelerator [13], the new n_TOF results on $^{151}\text{Sm}(n, \gamma)$ served to confirm such limitations and helped to refine the physical conditions of modern models of thermally-pulsing asymptotic giant-branch (TP-AGB) stars [34]. In the context of the classical *s*-process [33] the large cross section value measured at n_TOF in combination with the high-neutron density obtained from other neighboring branching nuclei [35] would imply an unrealistic temperature regime in excess of 4×10^8 K for the *s*-process operating during He-burning in TP AGB stars. On the other hand, more advanced hydrodynamical models for low-mass TP AGB stars [34] in combination with the measured cross section helped to constrain the thermal conditions of the He-shell flashes within a range of $T_8 = 2.5$ - 2.8 K, as well as to assess more consistently the *s*- and *p*-process contributions in the important Sm-Eu-Gd region [36].

$^{93}\text{Zr}(n, \gamma)$: temperature- and neutron-density conditions in AGB stars

The measurement of $^{93}\text{Zr}(n, \gamma)$ [37] was significantly more difficult despite of its relatively long half-life of 1.6 My (see Fig.2). Indeed, the capture cross-section of this Zr isotope is relatively small (~ 96 mb at 30 keV) and the sample enrichment was of only 20%. Similarly to the measurement of the ^{151}Sm -branching, two C_6D_6 detectors were used. In this case they were placed 9 cm upstream in order to reduce the background effect of in-beam γ -ray Compton scattering in the sample, which has a forward distribution

for high-energy γ -rays. The main limitation in this experiment was due to the background contribution beyond the \sim keV neutron-energy range arising from neutrons scattered in the sample and subsequently captured in the surrounding materials (see "setup" labeled spectrum in Fig.1 of Ref.[37]). As a consequence of this, the neutron-capture cross section could be determined only up to ~ 8 keV.

Including the new $^{93}\text{Zr}(n, \gamma)$ cross section measured at n_TOF in state-of-the-art models for thermally pulsing asymptotic-giant branch (TP-AGB) stars [38] allowed one to get a better insight about the origin of interstellar SiC grains in the CM2 (Mighei type) Murchison chondrite. Chondrites are meteorites that have not been modified by melting or differentiation processes in their parent bodies. These chondrites contain SiC grains, individual microcrystals that were already present in the protosolar nebula and which have survived from destructive processes in the interplanetary disk, in the parent bodies of their host chondrites, and also on their way to the Earth. Utilizing the cross section measured at n_TOF Lugaro and coworkers [39] found that the composition of the SiC grains arises mainly from low-mass ($1.5 M_\odot \leq M \leq 4 M_\odot$) TP-AGB stars, and ruled out the possibility of significant contributions from $\geq 4 M_\odot$ AGB stars, where the $^{22}\text{Ne}(\alpha, n)$ source is indeed more efficiently activated than in the lower-mass stars. A series of systematic capture-measurements on the stable $^{90-96}\text{Zr}$ -isotopes at n_TOF [40, 41, 42, 43, 44] in combination with new AGB models [45, 46] allowed to explore even more features about the origin of the SiC grains [47]. It was found that C-rich 1.25 - $4 M_\odot$ AGB stars with metallicities in the range of $Z=0.01$ - 0.03 reproduced well the variations of $^{90,91}\text{Zr}/^{94}\text{Zr}$ measured in the grains, as well as their Si-isotopic composition. The stellar metallicity was found to be the main parameter for explaining the correlation found between $^{92}\text{Zr}/^{94}\text{Zr}$ versus $^{29}\text{Si}/^{28}\text{Si}$ in these grains, rather than other effects such as stellar rotation [47]. In summary, the complete series of measurements on Zr isotopes allowed one to inspect important open questions about low-mass TP-AGBs, mainly related to the effects of the stellar mass, uncertainties in the ^{13}C -pocket and the interplay between metallicity and rotation [47]. Finally, the neutron-energy dependence of the cross-section measured at n_TOF [37], together with the abundance ratio $N(\text{Nb})/N(\text{Zr})$ observed in extrinsic S-type red-giant stars, allowed one to directly determine an effective value of the *s*-process temperature ($\lesssim 2.5 \times 10^8$ K) in evolved low-mass red-giant stars, independently of stellar evolution models [48]. As discussed in the latter work, if new experiments with improved accuracy (or equivalently with a reduced background in the keV neutron-energy region) could be performed, they would help to constrain even more the *s*-process temperature in red-giant TP-AGB stars (see $N(\text{Zr})/N(\text{Nb})$ error bars in Fig.1 of [48]).

$^{63}\text{Ni}(n, \gamma)$: constraining Cu-Ni-Zn inventory before CCSN explosion

A similar set-up of two C_6D_6 detectors placed ~ 9 cm upstream was used for the measurement of $^{63}\text{Ni}(n, \gamma)$ ($t_{1/2} =$

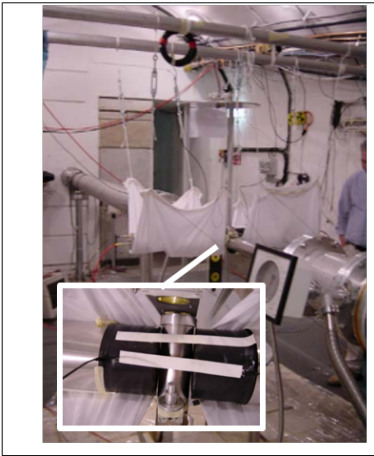
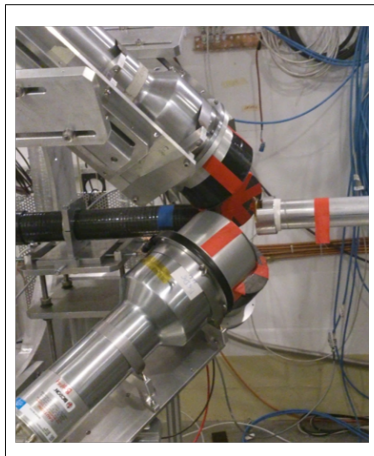
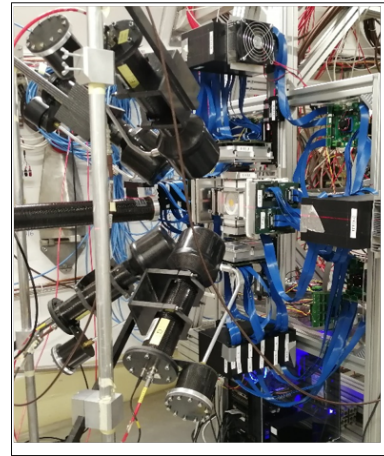
EAR1 $^{151}\text{Sm}(n,\gamma)$, 2001EAR1 $^{204}\text{Tl}(n,\gamma)$, 2015EAR1 $^{79}\text{Se}(n,\gamma)$, 2022

Fig. 3. Evolution of the capture set-up at EAR1, from left to right, two first-generation C-fiber based C_6D_6 detectors for the measurement of $^{151}\text{Sm}(n,\gamma)$ [24], four Bicorn C_6D_6 detectors with lead shields for the $^{204}\text{Tl}(n,\gamma)$ experiment [49] and four latest-generation C-fiber C_6D_6 detectors [50] plus the i-TED Compton array [51] for the $^{79}\text{Se}(n,\gamma)$ cross-section measurement [52].

101 yr) [53]. This experiment implied a step further in difficulty (see Fig. 2) mostly due to the low sample enrichment ($\sim 10\%$) and the reduced number of ^{63}Ni atoms in the sample. In spite of the excellent TOF (neutron-energy) resolution provided by the 185 m flight-path of EAR1, strong resonance-overlapping contributions in the keV energy range from the dominant ^{62}Ni content in the sample were difficult to disentangle from the capture-resonances of interest in ^{63}Ni (see Fig.2 in [53]). In short, the small cross section (~ 67 mb at 30 keV), the reduced number of atoms (10^{21} atoms, 112 mg) and the need to use a PEEK sample encapsulation contributed to a sample-scattered neutron-induced background which, in a similar way as in the measurement of $^{93}\text{Zr}(n,\gamma)$, limited the R-matrix analysis of the resolved resonances up to $E_n \sim 10$ keV. The $^{63}\text{Ni}(n,\gamma)$ measurement was complemented with the measurement of the stable ^{62}Ni [54] for a more reliable evaluation of the impact of these cross sections in the abundance ratio of $^{63}\text{Cu}:$ ^{65}Cu in massive stars ($M > 8M_\odot$), which is now predicted to be 40% smaller than what was accepted before on the basis of previous cross sections. This result allowed to reduce one of the main uncertainties for the abundances of ^{63}Cu , ^{64}Ni and ^{64}Zn in s-process rich ejecta of core collapse supernovae (CCSNe).

Recently, with the aim of having a fully consistent picture of the Ni-Cu-Zn abundances, a new measurement on $^{64}\text{Ni}(n,\gamma)$ [55] has been carried out at n_TOF and another one is planned on $^{56}\text{Fe}(n,\gamma)$ [56]. The measurement of $^{56}\text{Fe}(n,\gamma)$ was attempted during the Phase I of n_TOF [57] and, unfortunately, the in-beam γ -ray background (discussed in 2) severely constrained the quality of the data. Thanks to the new spallation target design [22] and the improved experimental conditions at EAR1 this cross section will be measured again in the coming years [56]. In the case of $^{64}\text{Ni}(n,\gamma)$, the main limitation for a previous measurement was due to the very low natural abundance

(0.92%) and the limited sample quantity available, which hindered a measurement in the past at EAR1. Thanks to the high flux and improved RF available now at the EAR2 station (20 m flight path) the $^{64}\text{Ni}(n,\gamma)$ cross section has been successfully measured in 2024.

$^{171}\text{Tm}(n,\gamma)$: solving rare-earth element anomalies in meteorites

The difficulty of the $^{63}\text{Ni}(n,\gamma)$ measurement was paralleled afterwards by the neutron-capture measurement of ^{171}Tm ($t_{1/2}=1.92$ yr) [58] (see Fig. 2). This experiment was performed at EAR1 utilizing an enlarged setup of four C_6D_6 detectors for higher detection efficiency. In spite of this, the covered neutron-energy range was limited further down to only ~ 1 keV owing to the much smaller number of atoms in the sample (2×10^{18} atoms). The more limited energy range (1 keV for ^{171}Tm versus 10 keV for ^{63}Ni) reflects that the $^{171}\text{Tm}(n,\gamma)$ experiment was indeed even more difficult than the previous one on ^{63}Ni discussed above. In this case, however, the drawback of the small sample quantity was counterbalanced to some extent by the rather large cross section (~ 400 mb at 30 keV), the high sample enrichment (98%) achieved at PSI via chemical purification and separation and the use of four C_6D_6 detectors, instead of the two units commonly used before. In addition, this is one of the relatively few cases where the TOF measurement can be conveniently complemented with an activation experiment which, in turn, became crucial for improving the measurement uncertainty down to 10% at a thermal energy of $kT = 30$ keV. The activation experiment was carried out at the SARAF facility [59]. The synergy in this unique combination contributed for building later the new local neutron-activation station (NEAR) at CERN n_TOF, which is discussed below in Sec.5.

The ^{171}Tm result helped to understand striking isotopic anomalies in rare-earth elements (REE) found in bulk SiC grains of the Murchison meteorite, particularly in three samples where the Yb-isotopic composition was analyzed [60]. The $^{171}\text{Yb}/^{172}\text{Yb}$ - and $^{173}\text{Yb}/^{172}\text{Yb}$ -isotopic ratios could be well reproduced after the new cross section measured at n.TOF and detailed modeling of the so-called third dredge-ups (TDUs) included in updated stellar models of low-mass stars [61]. SiC grains are thought to be synthesized after TDUs, during which by-products of nuclear burning occurring in stellar interiors, including carbon and s-process isotopes, are transported to the surface of the star. Another important consequence of understanding the SiC grain composition is that about one-half of the mass of the carbon-rich envelope is ejected into the interstellar medium (ISM) by winds of low-mass AGB stars has the isotopic composition fixed by the last TDU in such stars [39].

$^{204}\text{Tl}(n, \gamma)$: Shedding light on the origin of the heaviest s-only nucleus ^{204}Pb

^{204}Tl ($t_{1/2} = 3.78\text{yr}$) was the latest and most challenging s-process branching measured at EAR1 still with conventional C_6D_6 detectors [49] (see Fig.2). The sample contained just 2.66×10^{19} atoms of ^{204}Tl , representing an enrichment of only 4% with respect to the primary sample isotope ^{203}Tl . One of the main experimental difficulties was due to a ^{60}Co -contamination in the sample (373 kBq), which required the unconventional use of a 2 mm thick lead shielding in the front surface of each one of the four C_6D_6 detectors used for the experiment (see Fig.3). In addition, a rather high analysis threshold in deposited energy, of 600 keV (more than three times the usual value), was necessary to obtain an optimal signal-to-background ratio. The effect of this cut-off threshold could be nevertheless well accounted for thanks to the methodology developed in Ref.[62], which enables an accurate treatment of such experimental effects by means of realistic MC-calculations of the capture γ -ray cascades and detailed modeling of the experimental setup.

The synthesis of ^{204}Pb is shielded from r -process contributions by its stable isobar ^{204}Hg and thus, the split of the s-process path at ^{204}Tl is the responsible for the existence of all the ^{204}Pb that we find in the Solar System today. S-only nuclei are stable isotopes that, like ^{204}Pb , are entirely produced by the the s-process because they are shielded from r -process contributions by stable isobars. From ^{70}Ge to ^{204}Pb there exist ~ 30 s-only nuclei across the full nuclear chart. S-only nuclides are particularly relevant for benchmarking the performance of TP-AGB models at different metallicities, and for assessing the contribution of such stars to the chemical composition of our galaxy [11]. Previous studies [63] indicated the possible existence of unknown fragmentation mechanisms in the early Solar System affecting the abundance of the lead isotopes in Ivuna-type Chondrites (CI), with respect to the primordial Solar-System abundances. Supernovae are another hypothetical scenario that could potentially

affect the abundance of ^{204}Pb by means of p-process contributions [64,65]. As it turns out, addressing the primordial s-process origin of ^{204}Pb is relevant for dating the age of meteorites and their components formed in the first 5 Myr of the Solar System [66]. In particular, Pb-Pb cosmochronometry represents the state-of-the-art for determining the age of the Solar System by dating Calcium-Aluminum rich Inclusions (CAIs) in primitive meteorites [67]. Because ^{204}Pb is the only lead isotope which is exempt of radiogenic contributions from the decay of U- and Th-isotopes its abundance is used for relative normalization of the radiogenic components ($^{206,207}\text{Pb}$) in the Pb-Pb clock (see Eqs.(1-3) in [68]). In this way, ^{204}Pb becomes key for the unsurpassed $\sim 0.1\text{-}0.2$ Myr precision [69] of this cosmochronometer. New AGB nucleosynthesis calculations based on the cross section measured at n.TOF delivered ^{204}Pb abundances fully consistent with the latest solar-system abundance compilation by Lodders [70]. Within the quoted uncertainties this result ruled out the necessity of invoking fractionation mechanisms or any significant p-process contribution to the origin of ^{204}Pb . Reducing further the uncertainty on the s-process contribution to ^{204}Pb will require an accurate assessment of the thermal dependency of the β -decay rate of ^{204}Tl , which could be achieved in the next years in the framework of the PANDORA project [71].

Neutron-capture measurements on even more difficult s-process branchings utilizing samples with smaller number of atoms, lower enrichment and/or higher γ -ray activity, required the use and optimization of the second experimental area EAR2 at only 20 m from the spallation source. EAR2 delivers an instantaneous neutron flux, which is more than two orders-of-magnitude larger than the one available at EAR1 [28], making it a unique tool for suppressing the background contribution arising from the sample radioactivity. In addition, developing two new detection systems was necessary for the measurement of the next two, even more challenging, s-process branching nuclides ^{79}Se and ^{94}Nb , as described below.

$^{94}\text{Nb}(n, \gamma)$: disentangling Mo-isotopic anomalies in presolar SiC grains

The sample of ^{94}Nb ($t_{1/2} = 2 \times 10^4$ yr) contained 9×10^{18} atoms with only a 1% enrichment with respect to ^{93}Nb . In addition, the sample itself contained a ^{60}Co contamination of 10 MBq. These challenging features, exceeded the experimental capabilities of EAR1 (see Fig.2) and hindered the use of conventional C_6D_6 detectors (see Fig.4-left). The capture yield of the $^{94}\text{Nb}(n, \gamma)$ reaction could be successfully measured up to 10 keV of neutron energy implementing in EAR2 a new array of nine small-volume C_6D_6 (sTED) detectors [72,73] in a compact configuration around the sample (see Fig.4-right). The high instantaneous flux of EAR2 and the new set-up of detectors optimized for very high count-rate capability became crucial for overcoming the limitations imposed by the ^{60}Co sample activity[74].

EAR2, 2015

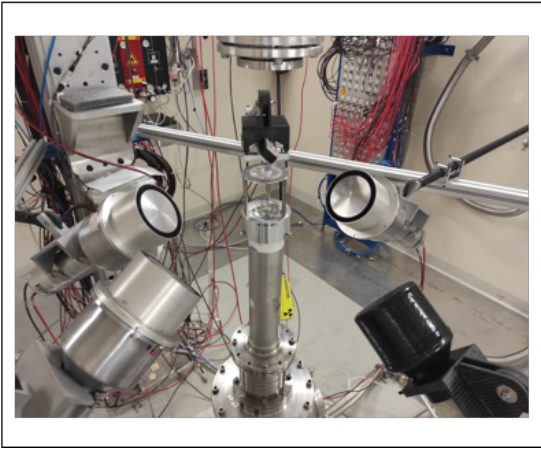
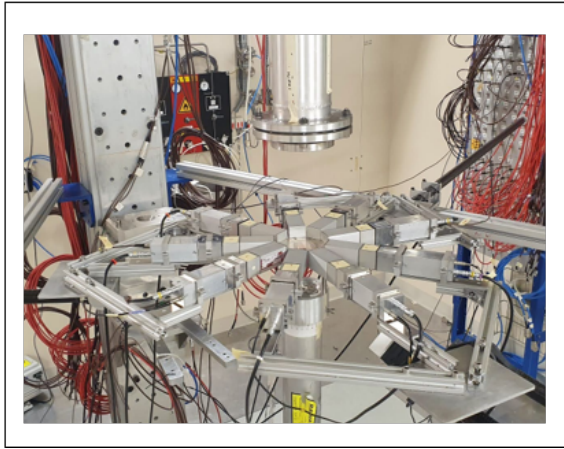
EAR2 $^{79}\text{Se}(n,\gamma)$ $^{94}\text{Nb}(n,\gamma)$, 2022

Fig. 4. Left: Conventional (large-volume) C_6D_6 detectors for capture measurements in EAR2. Notice that due to their large volume and the high neutron-flux the detectors had to be placed far from the sample in order to limit the count-rate per detector. Right: Upgraded setup with nine small volume C_6D_6 sTED detectors in a compact configuration surrounding the capture sample.

The neutron capture cross section measurement of ^{94}Nb at n_TOF and other stable Mo-isotopes discussed below, was motivated by the better understanding of AGB-contributions to the composition of mainstream SiC grains. Mainstream grains arise from low-mass C-rich AGB stars, as it is inferred from their isotopic signature [75] and the presence of SiC dust around such stars [76]. The heavy-element isotopic compositions of mainstream grains, like Mo-isotopes, is less affected by initial stellar composition or GCE effects as compared to light-elements ($A < 56$) and, for this reason, these elements are especially well suited for the study of AGB-stellar processes [77]. The Mo-isotopic abundances of mainstream grains were generally well reproduced by state-of-the-art AGB models, with the exception of ^{94}Mo [39]. There are several reasons that could affect the production of ^{94}Mo in stars, among them the branching at ^{94}Nb (see Fig.1 in [39]) leading to the formation of ^{94}Mo . This contribution is enhanced during the He-shell flashes of TP-AGB stars by the reduced ^{94}Nb half-life of only a few days at $T=3 \times 10^8$ K [78]. Uncertainties on the thermal-dependency of the ^{94}Nb β -decay rate, and the unknown $^{94}\text{Nb}(n,\gamma)$ neutron-capture cross section could be responsible of the observed discrepancy [39]. Low-mass TP-AGB models [39] predict about 4 times less ^{94}Mo than the relative quantities found in SiC grains (see Fig.8 in [39]). More recent low-mass AGB models with updated magnetohydrodynamics-based mixing schemes [79, 80] also yield an anomalous difference between predicted and measured ^{94}Mo abundance ratios in mainstream-SiC grains (see Fig.8 in [81]). Among the different isotopes involved, obviously neutron-capture on the unstable ^{94}Nb is the most difficult one to measure owing to the reasons highlighted above. However, uncertainties in the cross sections of the stable Mo-isotopes should not be ruled out and, for that reason, additional measurements on the stable $^{94-96}\text{Mo}$ isotopes have been recently carried out at

CERN n_TOF EAR1 [82,83]. Both the data-analysis of $^{94}\text{Nb}(n,\gamma)$ and $^{94-96}\text{Mo}(n,\gamma)$ are presently in progress and, once finalized, the uncertainties from the neutron-capture input data will be removed from this problem. It remains to be investigated if a different thermal dependency of the ^{94}Nb β -decay rate in the stellar plasma conditions could have a significant impact. Fortunately, the measurement of this decay-rate at high (stellar) temperature is precisely one of the first priorities of the future PANDORA project [71].

$^{79}\text{Se}(n,\gamma)$: temperature in Massive and AGB stars

Following the defined FOM (1), the most challenging s-process branching measured so far at CERN n_TOF via the time-of-flight technique is ^{79}Se (see Fig.2). ^{79}Se has a terrestrial half-life $t_{1/2} = 3.27(8) \times 10^5$ years [84] and the chemical element selenium itself has a melting point of only 494 K. Because of such low melting point an eutectic lead-selenide (PbSe) alloy [85], highly enriched in ^{208}Pb and ^{78}Se , was prepared at PSI with a total mass of 3.9 g [86] for subsequent activation at the high-flux reactor of ILL-Grenoble. The eutectic alloy was necessary to comply with safety regulations at ILL. The resulting activated sample contained only 2.7 mg of ^{79}Se , thus corresponding to an enrichment factor as low as 7×10^{-4} . In addition, the activity due to the γ -ray emitting decays of ^{75}Se and ^{60}Co from ineluctable impurities activated in the sample were of 5 MBq and 1.4 MBq, respectively. The complex data-analysis related to the use of the i-TED and sTED detectors in two different experimental areas is expected to be completed soon. We clearly observe a number resonances below ~ 1 keV related to neutron-capture on ^{79}Se , which means that it will be possible to provide the very first neutron-capture nuclear-input required for a proper interpretation of this important s-process branching point.

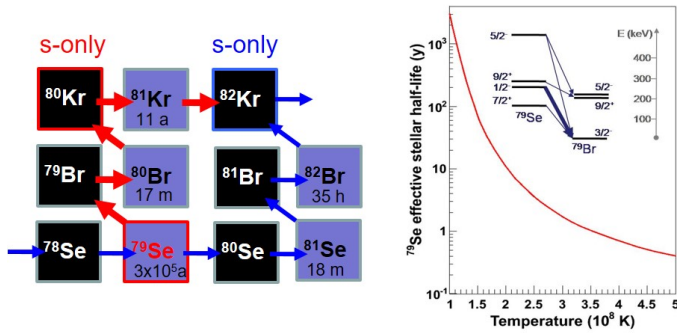


Fig. 5. Left: Part of the nuclear chart showing the s -process path at the branching in ^{79}Se . The β -decay towards s -only ^{80}Kr is strongly enhanced at higher stellar temperatures (red arrow) due to the population of the $1/2^-$ -isomeric state at low energy. Right: Effective half-life of ^{79}Se as a function of stellar temperature. The inset indicates levels involved.

The branching at ^{79}Se represents indeed one of the best cases to constrain the thermal conditions of the s -process [7,87]. Under stellar conditions, the half-life of ^{79}Se decreases to less than a year due to the population of the isomeric state at only 95.7 keV [88,78] (see Fig.5). Remarkably, this subtle nuclear-structure effect leads to final abundances for the s -only $^{80,82}\text{Kr}$ isotopes, which are strongly dependent upon the thermal conditions inside the star and the neutron-capture rate at ^{79}Se . Moreover, this neutron-capture cross section measurement could provide valuable information about s -process nucleosynthesis both in massive stars and in AGB stars because the s -process path induced by ^{79}Se is located in the transition region between weak (massive stars) and the main (low-mass AGBs) s -process contributions [87]. The stable end-products of the Se branching, the (s -only) Kr isotopes, have been well characterized in presolar graphite grains of the CM2 Murchison chondrite [89]. A striking property of these graphite grains is that their isotopic features depend on their density and, in fact, low-density grains are inferred to predominantly arise from CCSN explosions of massive stars [90,91], while high density ($>2.1\text{ g/cm}^3$) graphite grains are thought to mainly originate from C-rich AGB stars [89]. Therefore, once the experimental result from the neutron-capture cross section measurement carried out at n_TOF becomes available in the near future, a complete assessment of the thermal conditions both in AGB and massive stars will become possible by revisiting the readily available Kr-isotopic abundances from presolar low- and high-density graphite grains extracted from the Murchison meteorite.

4 Recent measurements on stable isotopes

Although neutron-capture cross-section measurements virtually exist for all stable isotopes of s -process interest, the related uncertainties are in most cases far from the $\pm 5\%$ uncertainty level required for s -process model calculation utilizing low-mass AGB models [61,92,93] and massive-star models [94,95]. Certainly, a large effort has been made

over the last years in order to access the challenging unstable s -process nuclei. However, it is worth emphasizing that many important facets of stellar nucleosynthesis in AGB- and massive stars still require significant effort with stable isotopes to reduce present uncertainties. This effort should focus on new measurements extending across the full energy range of astrophysical interest. In the following some recent examples are discussed in more detail.

4.1 S -process bottlenecks: $^{140}\text{Ce}(n,\gamma)$ and $^{209}\text{Bi}(n,\gamma)$

The neutron shell-closure effects along the s -process path are reflected in small capture cross sections, which lead to characteristic abundance peaks in the mass-regions of Sr, Y, Zr ($N=50$), Ba, La, Ce, Nd, Sm ($N=82$) and Pb, Bi ($N=126$). Because s -process bottleneck elements, in general, show-up prominently in spectroscopic observations of stellar atmospheres, from the observational point of view they can be accurately quantified in different types of stars, thus becoming good candidates for testing the details of the stellar models. However, cross section uncertainties for a large number of neutron-magic nuclei are still very sizable (see Fig.6 in [8] and Fig.1 in [96]). An uncertainty below $\sim 2\%$ [7,97] would be more convenient for a proper interpretation of the observed abundances and for exploring different aspects of low-mass AGB stars, such as the effect of metallicity [98] or the amount of ^{13}C in the pocket [99,34,13]. In practice, experiments with neutron-magic nuclei often present significant challenges due to their extremely low radiative capture cross sections. In some cases, these cross sections barely exceed a few millibarns at $kT = 30\text{ keV}$ [25]. Consequently, the radiative capture cross section can be up to three to four orders of magnitude smaller than the competing elastic scattering one within the stellar energy range of interest. In these scenarios, the high number of scattered neutrons may interact (promptly or after partial thermalisation) with materials in the surroundings of the experimental setup and detectors themselves. Such contaminant interactions emit radiation that contaminates the measurement and increases background levels. This phenomenon, referred to as neutron sensitivity, has driven advancements in detection systems. C_6D_6 detectors were introduced as a more suitable alternative to the C_6F_6 detectors commonly used in earlier studies [100]. At n_TOF, carbon-fibre based C_6D_6 scintillation detectors were initially developed [32] and progressively improved after many years of operation [50], thereby aiming at minimizing potential neutron sensitivity backgrounds (see Fig.3). These developments were of particular importance for achieving a high systematic accuracy in the measurement of neutron-magic isotopes [25]. Another source of background that may significantly affect these measurements is the in-beam γ -rays background, which becomes enhanced when measuring high-Z samples. In summary, the very-low capture cross sections of bottleneck isotopes makes their measurement very sensitive to any background contribution, and especial care needs to be taken in the design of the detection system and in the detectors themselves. Two recent s -process bottel-

neck measurements will be discussed here: ^{140}Ce [101] and ^{209}Bi [102].

^{140}Ce : the second *s*-process peak

For the measurement of the $^{140}\text{Ce}(n, \gamma)$ cross section [101] a highly enriched ^{140}Ce sample was produced at PSI. The sample mass was of 12.318 g (Ce-oxide) and the amount of ^{142}Ce was of only 0.6%. This enabled a high-resolution measurement at EAR1 covering a large neutron-energy range (up to 65 keV), thereby utilizing the conventional setup of four C_6D_6 detectors optimized for low neutron sensitivity backgrounds. The resulting Maxwellian averaged cross section was up to 40% higher than previously reported values and, in combination with low-mass AGB stellar models [103,61] a reduction of 20% in the *s*-process abundance of ^{140}Ce was obtained with respect to previous estimations.

The $^{140}\text{Ce}(n, \gamma)$ experiment was motivated by a discrepancy of 30% found between the Ce abundance predicted with AGB models and the quantity determined from spectroscopic observations of stars in the M22 globular cluster, for which the *s*-process pollution could be well isolated [104]. Interestingly, a good agreement was found between abundance predictions and observations for the neighbouring bottleneck elements: Ba, La, Nd and Sm (see Fig.11 in [104]). The new cross section leads to an even smaller predicted Ce-abundance (see Fig.1 in [101]), which does not solve this discrepancy and makes this problem even more intriguing. In addition, other independent activation experiments [105] provide a MACS value which differs significantly from the n_TOF result. This situation reflects the inherent difficulty in the measurement of bottleneck isotopes, which are characterized by their very low cross sections. As a consequence, a new activation experiment has been carried out at the new NEAR facility (see Sec.5) of n_TOF utilizing the same high-quality sample that was employed for the TOF experiment. For completeness, it is worth mentioning that some impact on the observed abundance may come from possible *i*-process contributions [106,107], that could be enhanced by a rather small $^{140}\text{Ba}(n, \gamma)$ cross section. Obviously, this contribution cannot resolve the discrepancies in the MACS determined from different experiments. Both theoretical, experimental and (probably) observational efforts seem to be required at this stage in order to shed some light on this interesting case.

^{209}Bi : the third *s*-process peak

Bismuth is the heaviest element produced by the *s*-process in low-mass AGB stars, it is monoisotopic ($A=209$), and its abundance in the Solar System is relatively well known [70]. The $^{209}\text{Bi}(n, \gamma)$ cross section was measured at CERN n_TOF EAR1 in 2001[25] with a set-up similar to the one shown in Fig.3-left. Together with the measurement of the neighboring lead isotopes $^{204,206,207}\text{Pb}$ [108,109,110], relevant information could be obtained for the study of

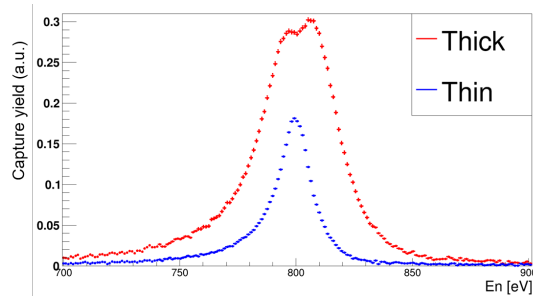


Fig. 6. Comparison of the capture yields measured at n_TOF EAR2[102] for the first capture-resonance in $^{209}\text{Bi}+n$ with a thick and a thin sample.

the termination region of the *s*-process path (see previous references and Sec.5 in Ref.[111]). In particular, rather accurate abundance constraints could be derived for the *r*-process contribution to ^{209}Bi (see Fig.5 in [111]) via the so-called *r*-process residuals ($N_r = N_{\odot} - N_s$), given that the corresponding *s*-process abundance was well determined from the measured cross section and TP-AGB stellar models (see [25] and references therein) and the fact that the solar system abundance of Bi (N_{\odot}^{Bi}) is relatively well known ($\sim 7\%$ relative uncertainty) from the isotopic analysis of CI-chondrites [70]. In turn, the *r*-process residuals analysis helped to qualify or reject some of the former nuclear-mass models utilized in *r*-process model calculations [112,111].

However, despite efforts in reducing the intrinsic neutron-sensitivity of the detection apparatus, the first measurement of ^{209}Bi at n_TOF encountered many difficulties due to the aforesaid in-beam γ -ray background, which was significantly enhanced by the high-Z (83) of the sample. This background was indeed largest in the ~ 10 keV neutron-energy range, which hindered the observation of some resonances and reduced significantly the statistical accuracy in many of them. With the new improved experimental conditions discussed in Sec.2 a new measurement of $^{209}\text{Bi}(n, \gamma)$ was successfully carried out in 2024 at EAR2[102]. Preliminary results indicate that with the new measurement one could obtain an improvement in both the covered energy range and the number (and statistical accuracy) of resonances observed. In addition, the high-flux at EAR2 enabled the measurement of two independent Bismuth samples, with two different thicknesses, which permitted a better assessment of multiple-scattering and neutron-sensitivity effects. These two experimental effects are of particular importance in the case of broad *s*-wave resonances (see Fig.6).

4.2 $^{28-30}\text{Si}(n, \gamma)$: disentangling Si-Ti-Mg isotopic anomalies in mainstream SiC grains

Even for the most abundant and best known mainstream SiC presolar grains, already discussed here in the context of the ^{94}Nb -branching in Sec.3, the mass and metallicity properties of their progenitor AGB stars are still quite ambiguous [113,114]. Modern galactic chemo-dynamical

models indicate that $M \sim 2M_{\odot}$ and $Z \sim Z_{\odot}$ C-rich AGB stars seem to be the main progenitors of these SiC grains in our Solar System [113], whereas previous studies rather point to AGB stars with masses up to $4 M_{\odot}$ and $Z \sim 2Z_{\odot}$ [114]. In turn, the mass- and metallicity-distributions of the AGB-star population is of fundamental relevance for s-process nucleosynthesis and for understanding the chemical evolution of our galaxy. As discussed before in the context of the ^{94}Nb branching in Sec.3, heavy element isotopic compositions of mainstream grains, like Zr or Mo, can help to avoid effects related to the ISM composition or the imprints of GCE. In practice, improving current uncertainties in the neutron-capture cross sections of the light Si-isotopes, commonly used for the isotopic-classification and interpretation of SiC grains [77], may also contribute to disentangle possible imprints of the ISM composition in the formation of these grains from the intrinsic nucleosynthesis contribution of the C-rich AGB progenitor.

Experimentally, neutron-capture measurements on silicon isotopes are challenging owing to their very small neutron capture cross section. A further difficulty is the significant direct capture contribution expected in these light nuclei, which can only be estimated theoretically or inferred from the thermal neutron-capture value if it is precisely known. Latest neutron-capture measurements on the Si-isotopes were rather inconclusive regarding the interpretation of the isotopic-composition of mainstream SiC grains, with important shifts with respect to expectations found for $^{29,30}\text{Si}$ [115]. In an effort to improve this situation a new series of measurements on $^{28,29,30}\text{Si}(n, \gamma)$ were carried out at n_TOF utilizing highly enriched samples, state-of-the-art C_6D_6 detectors and both EAR1 and EAR2 experimental areas [116]. The two independent measurements in EAR1 and EAR2 with complementary setups (four C-fiber C_6D_6 and nine sTED-detector array) allows one to keep under control systematic effects related to multiple-scattering and other experimental effects. For $^{30}\text{Si}(n, \gamma)$ resonances have been observed up to several hundreds keV and the MACS at 30 keV seems to be dominated by the first strong resonances in the 5-15 keV energy range. Fig.7 displays an example of the excellent statistical quality of the data, showing a capture yield that is remarkably smaller than the values predicted by evaluations.

5 Present limits and new horizons

Some of the main persistent issues and limitations in the field of neutron-capture experiments for s-process studies are discussed in this section. A synopsis is also given on current plans for overcoming such limitations in the coming years at n_TOF, as well as new envisioned ideas for advancing further in more longer-term plan (coming decades).

The very first limitation in most of the challenging cases shown in Fig.2 starts with the quality of the capture sample itself. In spite of efforts and resources invested in manufacturing the best suitable samples for capture

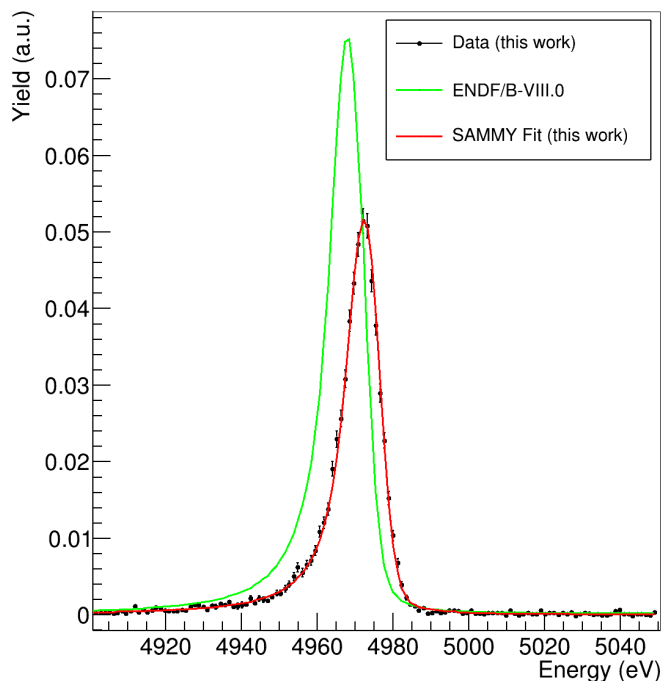


Fig. 7. R-matrix fit and its expected shape based on the ENDF/B-VIII.0 parameters of the first resonance in $^{30}\text{Si}+n$ measured in EAR1.

experiments, in most cases their final quality and composition still represents one of the main restrictions. Let us take as example the most challenging $^{79}\text{Se}(n, \gamma)$ case discussed in Sec.3. Having a chemically (Se) pure sample, instead of a lead-selenide eutectic alloy, would represent a remarkable advantage. All backgrounds arising from neutron-scattering in the lead content would be removed and also, the ^{60}Co contamination in the measured sample (1.4 MBq) arose from traces of ^{nat}Co in the highly enriched ^{208}Pb raw material used for producing the eutectic PbSe alloy [86]. It is technically feasible to obtain a radiochemically pure sample of Selenium, such as the sample prepared at PSI [117] for the measurement of the ^{79}Se half-life [84]. However, the cost and resources required to obtain a sufficient number of ^{79}Se atoms ($>10^{18}$) for a TOF experiment would be prohibitive. A radio-isotopically pure sample of ^{79}Se would enable a further huge improvement in reducing backgrounds during the measurement, and probably would lead to an experimental determination of the neutron-capture cross section in the full energy range of astrophysical interest ($\sim 1 \text{ eV} - 100 \text{ keV}$). This additional purification step would require the use of a dedicated mass-separator and the final sample amount would strongly depend on the design of such apparatus and the initial quantity and quality of material available. Only a few laboratories worldwide are equipped with the instrumentation and knowledge required to handle and produce such samples [118]. A big coordination effort is being pursued in the context of the SANDA [119] and its follow-up APRENDE project [120], as well as by the International Nuclear Target Development Society [121]. An off-line iso-

top separator for such purpose has been envisaged at PSI, which would be well suited for the production of radio-isotopically pure samples with sufficient amounts, in suitable backings and free from oxides (see also related discussion in Ref.[122]).

One of the main limitations in TOF experiments that becomes apparent after analyzing the seven *s*-process branching examples discussed in Sec.3 (see Fig.2) is the neutron-energy range efficiently covered in such experiments. The white neutron-flux spectrum and low duty-cycle of n_TOF allows one to fully cover the 1 eV to 100 keV energy range of interest for *s*-process studies. However, that wide energy range could only be analyzed in the very first $^{151}\text{Sm}(n, \gamma)$ experiment (see Fig.1 in Ref.[24]). For all other *s*-process branching cases discussed in Sec.3, the upper data-analysis limit was between 1 keV and 10 keV, thus missing an important (if not the most important) part of the stellar spectrum. In many cases the energy range beyond 10 keV corresponds already to the unresolved resonance region (URR) and thus, if the signal-to-background ratio is not adequate, it becomes increasingly difficult and uncertain to reliably extract the cross section. In such cases average resonance parameters were determined in the measured (low-energy) range, and a simulation of random-resonance sequences was computed to determine the MACS at higher kT thermal energies (see e.g.[58,49]).

Improving the experimental background conditions, or enhancing further the sensitivity of the detection apparatus with ideas similar to i-TED [51,123] or sTED [72] could help to overcome this limitation in future experiments. Presently, there are several efforts in this direction. A new (enlarged) version of the sTED array is being developed for experiments at both EAR1 and EAR2, thereby exploring a new technique with intermediate detection efficiencies [124]. Moreover, a new version of the sTED-detector array based on stilbene-d₁₂ organic crystals instead of C₆D₆ cells [72], the so-called Stilbene-d₁₂ deTector ARray (STAR), has been designed and is already under construction [73]. The use of even smaller detection volumes ($25 \times 25 \times 50 \text{ mm}^3$) of higher intrinsic detection efficiency than liquid C₆D₆ is expected to enhance further the signal-to-background ratio in future experiments at EAR2. It is foreseen that STAR will be commissioned in 2026 and operational for first capture experiments in 2028, after the third long shutdown (LS3) of CERN. A complementary and alternative effort, that in some specific cases may help to overcome the aforementioned limitation in neutron-energy range is the new NEAR activation station [125,126], located at only 3 m from the spallation source (see Fig.8). With an average flux of $\sim 5 \times 10^7 \text{ n/cm}^2/\text{s}$ this new facility will open the possibility to conduct, when feasible, activation experiments with quasi-Maxwellian neutron distributions spanning from $\sim \text{keV}$ up to $\sim 100 \text{ keV}$. The precise value of kT will be determined by the chosen (variable) thickness of a boron carbide (B₄C) filter embedding the sample under study [125]. A commissioning of the NEAR station and a flux characterization has been already carried out [125] and its main features and ancillary equipment are described in detail in Ref.[127]. A

Be moderator directly attached to one side of the spallation target will be installed during 2025, which will allow to improve the quality of the quasi-Maxwellian neutron spectrum significantly (see insets in Fig.8).

The potential of NEAR for new activation measurements on unstable nuclei will be boosted by the availability of the nearby ISOLDE facility and the large yields that can be produced therein [128,129]. Radioisotopically pure samples with sufficient number of atoms ($\sim 10^{15-16}$) will be produced at ISOLDE for the envisaged activation experiments at n_TOF NEAR. At present, this approach is already being tested with the production of a ^{135}Cs sample at ISOLDE utilizing General Purpose Separator (GPS) [130]. Once the sample becomes available, the activation measurement at NEAR is foreseen for 2026 [131]. For the measurement of isotopes leading to short-lived activated products the CYCLING (CYCLic activation station for (N,G) experiments) is being prepared and background characterization measurements at NEAR have been already carried out utilizing active (NaI-scintillation) detectors [132]. With NEAR and NEAR-CYCLING, in combination with the enhanced sample-production capabilities of ISOLDE, ILL and PSI, we expect to expand the number of (n, γ) cases of astrophysical interest in the coming years, as well as to provide complementary information in the 10-100 keV energy range, for those TOF experiments in EAR1 or EAR2 that are technically restricted to maximum neutron-energies of $\sim 10 \text{ keV}$. Several *s*-process cases to be tackled in the future at NEAR have been discussed already in Ref.[23,96], including some direct measurements for *i*-process studies.

In the longer term, the n_TOF collaboration is planning to expand further on the large potential of the activation technique and on its complementarity for many TOF experiments in EAR1 and EAR2. In this respect, an expression of interest for a new high-flux activation station n_ACT has been prepared [133]. The latter would be built at the SPS Beam Dump Facility (BDF) [134], where ultra-high neutron fluxes will be produced. n_ACT would allow to strategically profit such high neutron fluence. Preliminary designs for n_ACT [133] predict about three orders of magnitude higher fluxes than what is presently achievable at NEAR. Again, in combination with radio-isotopically pure samples from ISOLDE, this new facility may open-up the possibility to access for the first time direct (activation) measurements on samples available in minor quantities, including some neutron-rich unstable nuclei in the *i*-process path.

Finally, regarding possible long-term advancements, it is worth discussing here the concept of direct neutron-capture measurements in inverse kinematics with a stationary neutron target, which was proposed in Refs.[135,136]. If feasible, this novel methodology will allow one to overcome experimental difficulties that have been discussed above, mainly those connected with the production of the capture sample, the relatively large number of atoms required, the half-life of the isotope of interest and the radioactivity of the sample itself. Other additional aspects related to detector-sensitive backgrounds could

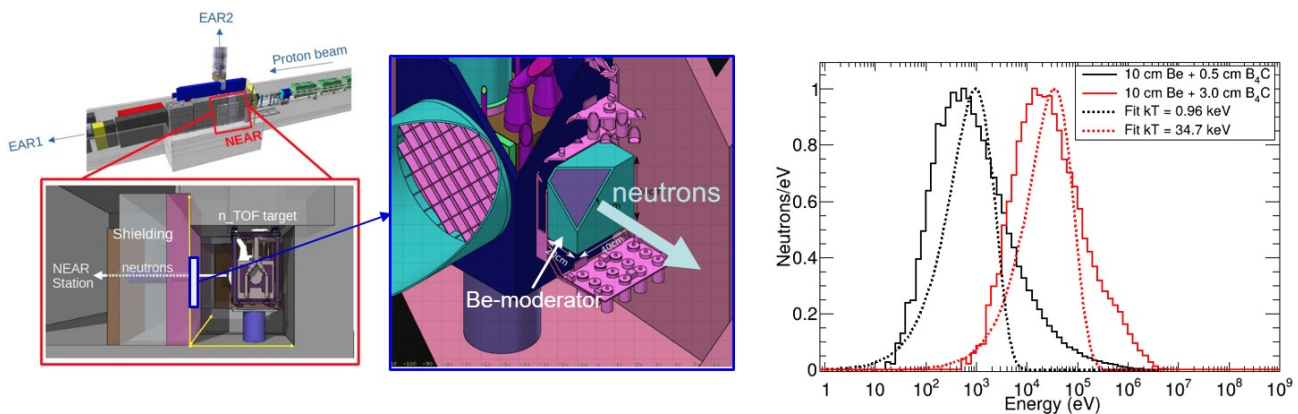


Fig. 8. Drawings showing the location and different elements of the new NEAR station (left) and some quasi-Maxwellian neutron distributions obtained via MC-Simulation for different B₄C-filter thicknesses, leading to mean kT values of about 1 keV and 35 keV.

be significantly improved as well. This new technique involves the combination of three main elements, namely, a radioactive ion-beam facility (preferably ISOL-type for low-energy secondary beams in the stellar energy range of interest 50-500 keV), a suitable low-energy storage ion-ring, and a heavily moderated spallation neutron source to drive the free neutron-gas target. A neutron target demonstrator is already being developed at Los Alamos Neutron Science Center (LANSCE) [137] and there are plans to demonstrate its performance in the coming years with a proof-of-concept experiment utilizing single-pass stable-beam experiments [137]. At TRIUMF-Vancouver, there are also plans to exploit the high-intensity ISOL yields of the ARIEL facility in combination with a low-energy storage ring (TRISR) and an alternative option based on compact neutron generators for the static neutron target is under study [8].

Interestingly, most of the three basic elements required for the new methodology are readily available at CERN, or at least a large expertise exists with them. On the one hand, ISOLDE would be an ideally well suited installation for the production of low-energy neutron-rich nuclei with high yields for this application. On the other hand, the 25 years of n_TOF experiment have led to a great expertise in the design and operation of spallation-targets [138] (see Fig.1), including also the new plans at the SPS-BDF facility [133]. A low-energy storage ring, the Test Storage Ring (TSR) was built [139] and operated at MPI-Heidelberg, with later (unsuccessful) plans to install it at HIE-ISOLDE [140]. More recently, in the framework of the EPIC ISOLDE upgrade, there is a renewed interest for a new Isolde Storage Ring (ISR), which could become a reality at CERN in the coming decade.

In summary, after 25 years of stunning developments and fascinating results at CERN n_TOF, new disruptive approaches like the inverse-kinematics concept could represent in the long-term future a new paradigm in this field. This new methodology could open the possibility of measuring the few remaining *s*-process branching nuclei, most of the isotopes in the *i*-process path and even approach the neighborhood of the *r*-process path.

Acknowledgments

CDP acknowledges Nan Liu (Boston University) for very helpful comments and suggestions. The authors acknowledge support from all the funding agencies of participating institutions. Part of this work was supported by the European Research Council (ERC) under the European Union’s Horizon 2020 research and innovation programme (ERC-COG Nr. 681740 and ERC-STG Nr.677497), European H2020-847552 (SANDA), the MCIN/AEI 10.13039/501100011033 under grants Severo Ochoa CEX2023-001-292-S, PID2022-138297NB-C21, PID2019-104714GB-C21, FPA2017-83946-C2-1-P, FIS2015-71688-ERC, FPA2016-77689-C2-1-R, RTI2018-098117-B-C21, PGC2018-096717-B-C21, PID2021-123100NB-I00 funded by MCIN/AEI 10.13039/501100011033/FEDER, UE, PCI2022-135037-2 funded by MCIN/AEI 10.13039/501100011033 and EU-NextGenerationEU/PRTR.

For the purpose of open access, the corresponding author has applied a Creative Commons Attribution (CC BY-NC-ND 4.0) license to any Author Accepted Manuscript version arising from this submission.

References

1. E. M. Burbidge et al. Synthesis of the elements in stars. *Reviews of Modern Physics*, 29:547–650, Oct 1957.
2. A. G. W. Cameron. On the origin of the heavy elements. *Astronomical Journal*, 62:9–10, Feb 1957.
3. R. L. Macklin et al. Neutron Capture in Tin Isotopes at Stellar Temperatures. *Nature*, 194(4835):1272, Jun 1962.
4. R. L. Macklin et al. Neutron Capture in the Samarium Isotopes and the Formation of the Elements of the Solar System. *Nature*, 197(4865):369–370, Jan 1963.
5. R. L. Macklin and J. H. Gibbons. Capture-Cross-Section Studies for 30-220-keV Neutrons Using a New Technique. *Physical Review*, 159:1007–1012, July 1967.
6. J. H. Gibbons and R. L. Macklin. Neutron Capture and Stellar Synthesis of Heavy Elements. *Science*, 156(3778):1039–1049, May 1967.

7. F. Käppeler et al. The s process: Nuclear physics, stellar models, and observations. *Reviews of Modern Physics*, 83(1):157–194, Jan 2011.
8. I. Dillmann et al. Measuring neutron capture cross sections of radioactive nuclei: From activations at the FZK Van de Graaff to direct neutron captures in inverse kinematics with a storage ring at TRIUMF. *European Physical Journal A*, 59(5):105, May 2023.
9. C. Travaglio et al. Galactic Evolution of Sr, Y, And Zr: A Multiplicity of Nucleosynthetic Processes. *ApJ*, 601(2):864–884, February 2004.
10. S. Bisterzo et al. The branchings of the main s-process: their sensitivity to α -induced reactions on ^{13}C and ^{22}Ne and to the uncertainties of the nuclear network. *MNRAS*, 449(1):506–527, May 2015.
11. N. Prantzos et al. Chemical evolution with rotating massive star yields II. A new assessment of the solar s- and r-process components. *MNRAS*, 491(2):1832–1850, January 2020.
12. S. Bisterzo et al. Galactic Chemical Evolution and Solar s-process Abundances: Dependence on the ^{13}C -pocket Structure. *ApJ*, 787(1):10, May 2014.
13. C. Arlandini et al. Neutron Capture in Low-Mass Asymptotic Giant Branch Stars: Cross Sections and Abundance Signatures. *ApJ*, 525(2):886–900, November 1999.
14. S. Goriely. Uncertainties in the solar system r-abundance distribution. *A&A*, 342:881–891, February 1999.
15. M. Arnould et al. The r-process of stellar nucleosynthesis: Astrophysics and nuclear physics achievements and mysteries. *Phys. Rep.*, 450(4-6):97–213, September 2007.
16. C. Rubbia et al. A High Resolution Spallation Driven Facility at the CERN-PS to Measure Neutron Cross Sections in the Interval from 1 eV to 250 MeV : a Relative Performance Assessment. Technical report, CERN-LHC-98-002-EET-Add.1; <https://cds.cern.ch/record/363828>, 1998.
17. F. Gunsing et al. The Neutron Time-Of-Flight Facility n_TOF At CERN: Phase II. In F. D. McDaniel and B. L. Doyle, editors, *Application of Accelerators in Research and Industry: Twenty-First International Conference*, volume 1336 of *American Institute of Physics Conference Series*, pp. 547–551. AIP, June 2011.
18. C. Guerrero et al. Performance of the neutron time-of-flight facility n_TOF at CERN. *European Physical Journal A*, 49:27, February 2013.
19. N. Colonna et al. Neutron physics with accelerators. *Progress in Particle and Nuclear Physics*, 101:177–203, July 2018.
20. C. Domingo-Pardo et al. The neutron time-of-flight facility n_TOF at CERN Recent facility upgrades and detector developments. In *Journal of Physics Conference Series*, volume 2586 of *Journal of Physics Conference Series*, pp. 012150. IOP, September 2023.
21. G. Lorusso et al. Time-energy relation of the n_TOF neutron beam: energy standards revisited. *Nuclear Instruments and Methods in Physics Research A*, 532(3):622–630, October 2004.
22. R. Esposito et al. Design of the third-generation lead-based neutron spallation target for the neutron time-of-flight facility at CERN. *Physical Review Accelerators and Beams*, 24(9):093001, September 2021.
23. J. Leredegui-Marco et al. New perspectives for neutron capture measurements in the upgraded CERN-n_TOF Facility. In *European Physical Journal Web of Conferences*, volume 284 of *European Physical Journal Web of Conferences*, pp. 01028, July 2023.
24. S. Marrone et al. A low background neutron flux monitor for the n_TOF facility at CERN. *Nuclear Instruments and Methods in Physics Research A*, 517(1-3):389–398, Jan 2004.
25. C. Domingo-Pardo et al. New measurement of neutron capture resonances in Bi209. *Physical Review C*, 74(2):025807, August 2006.
26. E. Chiaveri et al. Present status and future programs of the n_TOF experiment. In *European Physical Journal Web of Conferences*, volume 21 of *European Physical Journal Web of Conferences*, pp. 03001, February 2012.
27. S. Barros et al. Optimization of n_TOF-EAR2 using FLUKA. *Journal of Instrumentation*, 10(9):P09003, September 2015.
28. J. Leredegui-Marco et al. Geant4 simulation of the n_TOF-EAR2 neutron beam: Characteristics and prospects. *European Physical Journal A*, 52(4):100, April 2016.
29. S. Lo Meo et al. GEANT4 simulations of the n_TOF spallation source and their benchmarking. *European Physical Journal A*, 51:160, December 2015.
30. P. Koehler. Comparison of white neutron sources for nuclear astrophysics experiments using very small samples. *Nuclear Instruments and Methods in Physics Research Section A: Accelerators, Spectrometers, Detectors and Associated Equipment*, 460(2):352–361, 2001.
31. M. Lugaro et al. The s Process and Beyond. *Annual Review of Nuclear and Particle Science*, 73:315–340, September 2023.
32. R. Plag et al. An optimized C_6D_6 detector for studies of resonance-dominated (n,γ) cross-sections. *Nuclear Instruments and Methods in Physics Research A*, 496:425–436, January 2003.
33. F. Käppeler et al. s-process nucleosynthesis-nuclear physics and the classical model. *Reports on Progress in Physics*, 52(8):945–1013, August 1989.
34. R. Gallino et al. Evolution and Nucleosynthesis in Low-Mass Asymptotic Giant Branch Stars. II. Neutron Capture and the S-Process. *ApJ*, 497(1):388–403, April 1998.
35. J. Best et al. s-process branchings at ^{151}Sm , ^{154}Eu , and ^{163}Dy . *Phys. Rev. C*, 64(1):015801, July 2001.
36. S. Marrone et al. Measurement of the $\text{Sm}151(n,\gamma)$ cross section from 0.6 eV to 1 MeV via the neutron time-of-flight technique at the CERN n_TOF facility. *Phys. Rev. C*, 73(3):034604, March 2006.
37. G. Tagliente et al. The $^{93}\text{Zr}(n,\gamma)$ reaction up to 8 keV neutron energy. *Physical Review C*, 87(1):014622, Jan 2013.
38. O. Straniero et al. Evolution and Nucleosynthesis in Low-Mass Asymptotic Giant Branch Stars. I. Formation of Population I Carbon Stars. *ApJ*, 478(1):332–339, March 1997.
39. M. Lugaro et al. Isotopic compositions of strontium, zirconium, molybdenum, and barium in single presolar SiC grains and asymptotic giant branch stars. *The Astrophysical Journal*, 593(1):486–508, aug 2003.
40. G. Tagliente et al. Experimental study of the $\text{Zr}91(n,\gamma)$ reaction up to 26 keV. *Phys. Rev. C*, 78(4):045804, October 2008.
41. G. Tagliente et al. Neutron capture cross section of $\text{Zr}90$: Bottleneck in the s-process reaction flow. *Phys. Rev. C*, 77(3):035802, March 2008.

42. G. Tagliente et al. The $Zr92(n,\gamma)$ reaction and its implications for stellar nucleosynthesis. *Phys. Rev. C*, 81(5):055801, May 2010.
43. G. Tagliente et al. $^{96}Zr(n,\gamma)$ measurement at the n_TOF facility at CERN. *Phys. Rev. C*, 84(5):055802, November 2011.
44. G. Tagliente et al. Neutron capture on Zr94: Resonance parameters and Maxwellian-averaged cross sections. *Phys. Rev. C*, 84(1):015801, July 2011.
45. M. Lugaro et al. Reaction Rate Uncertainties and the Production of ^{19}F in Asymptotic Giant Branch Stars. *ApJ*, 615(2):934–946, November 2004.
46. A. I. Karakas et al. Nucleosynthesis Predictions for Intermediate-Mass Asymptotic Giant Branch Stars: Comparison to Observations of Type I Planetary Nebulae. *ApJ*, 690(2):1130–1144, January 2009.
47. M. Lugaro et al. The Impact of Updated Zr Neutron-capture Cross Sections and New Asymptotic Giant Branch Models on Our Understanding of the S Process and the Origin of Stardust. *ApJ*, 780(1):95, January 2014.
48. P. Neyskens et al. The temperature and chronology of heavy-element synthesis in low-mass stars. *Nature*, 517(7533):174–176, Jan 2015.
49. A. Casanovas-Hoste et al. Shedding Light on the Origin of ^{204}Pb , the Heaviest s -Process-Only Isotope in the Solar System. *Phys. Rev. Lett.*, 133(5):052702, July 2024.
50. F. Mastinu et al. New C_6D_6 detectors: reduced neutron sensitivity and improved safety. Technical report, n_TOF-PUB-2013-002 ; CERN-n_TOF-PUB-2013-002; <https://cds.cern.ch/record/1558147/>, 2021.
51. C. Domingo-Pardo. i-TED: A novel concept for high-sensitivity (n,γ) cross-section measurements. *Nuclear Instruments and Methods in Physics Research A*, 825:78–86, July 2016.
52. J. Lerendegui-Marco et al. New detection systems for an enhanced sensitivity in key stellar (n,γ) measurements. In *European Physical Journal Web of Conferences*, volume 279 of *European Physical Journal Web of Conferences*, pp. 13001. EDP, September 2023.
53. C. Lederer et al. $^{197}Au(n,\gamma)$ - towards a new standard for energies relevant to stellar nucleosynthesis. *Journal of Physics Conference Series*, 337(1):012045, February 2012.
54. C. Lederer et al. $Ni62(n,\gamma)$ and $Ni63(n,\gamma)$ cross sections measured at the n_TOF facility at CERN. *Physical Review C*, 89(2):025810, February 2014.
55. G. Tagliente et al. Measurement of the neutron capture cross section of ^{64}Ni . Technical report, CERN-INTC-2022-033 ; INTC-P-208-ADD-1; <https://cds.cern.ch/record/2809947/>, 2022.
56. A. Casanovas et al. New high-resolution measurement of $^{56}Fe(n,g)$ at n_TOF-EAR1 for Nuclear Astrophysics and Nuclear Technology (CERN-INTC-2024-069 ; INTC-P-721) <https://cds.cern.ch/record/2912234/>. Technical report, CERN, 2024.
57. J.L. Tain et al. The role of Fe and Ni for s-process nucleosynthesis in the early Universe and for innovative nuclear technologies (CERN-INTC-2006-012 ; INTC-P-208) <https://cds.cern.ch/record/923161/>. Technical report, CERN, 2006.
58. C. Guerrero et al. Neutron Capture on the s -Process Branching Point Tm 171 via Time-of-Flight and Activation. *Physics Review Letters*, 125(14):142701, October 2020.
59. M. Paul et al. Reactions along the astrophysical s-process path and prospects for neutron radiotherapy with the Liquid-Lithium Target (LiLiT) at the Soreq Applied Research Accelerator Facility (SARAF). *European Physical Journal A*, 55(3):44, March 2019.
60. Q.-Z. Yin et al. Signatures of the s-Process in Presolar Silicon Carbide Grains: Barium through Hafnium. *ApJ*, 647(1):676–684, August 2006.
61. S. Cristallo et al. Evolution, Nucleosynthesis, and Yields of Low-mass Asymptotic Giant Branch Stars at Different Metallicities. II. The FRUITY Database. *ApJS*, 197(2):17, December 2011.
62. U. Abbondanno et al. Neutron capture cross section measurement of ^{151}Sm at the cern neutron time of flight facility (n_tof). *Physical Review Letters*, 93:161103, Oct 2004.
63. A. J. González et al. Design of the PET-MR system for head imaging of the DREAM Project. *Nuclear Instruments and Methods in Physics Research A*, 702:94–97, February 2013.
64. T. Rauscher et al. Nucleosynthesis in Massive Stars with Improved Nuclear and Stellar Physics. *ApJ*, 576(1):323–348, September 2002.
65. M. Pignatari et al. The production of proton-rich isotopes beyond iron: The γ -process in stars. *International Journal of Modern Physics E*, 25(4):1630003–232, April 2016.
66. J. N. Connelly et al. Chronology of the Solar System’s Oldest Solids. *ApJ*, 675(2):L121, March 2008.
67. J. N. Connelly et al. The Absolute Chronology and Thermal Processing of Solids in the Solar Protoplanetary Disk. *Science*, 338(6107):651, November 2012.
68. J. N. Connelly et al. Pb-Pb chronometry and the early Solar System. *Geochim. Cosmochim. Acta*, 201:345–363, March 2017.
69. Y. Amelin et al. Modern U-Pb chronometry of meteorites: Advancing to higher time resolution reveals new problems. *Geochim. Cosmochim. Acta*, 73(17):5212–5223, September 2009.
70. K. Lodders. Relative Atomic Solar System Abundances, Mass Fractions, and Atomic Masses of the Elements and Their Isotopes, Composition of the Solar Photosphere, and Compositions of the Major Chondritic Meteorite Groups. *Space Sci. Rev.*, 217(3):44, April 2021.
71. D. Mascalci et al. A new approach to β -decays studies impacting nuclear physics and astrophysics: The PAN-DORA setup. In *European Physical Journal Web of Conferences*, volume 279 of *European Physical Journal Web of Conferences*, pp. 06007, September 2023.
72. V. Alcayne et al. A Segmented Total Energy Detector (sTED) optimized for (n,γ) cross-section measurements at n_TOF EAR2. *Radiation Physics and Chemistry*, 217:111525, April 2024.
73. J. Balibrea-Correa et al. Towards a new generation of solid total-energy detectors for neutron-capture time-of-flight experiments with intense neutron beams. *Nuclear Instruments and Methods in Physics Research A*, 1072:170110, March 2025.
74. J. Balibrea-Correa et al. Pushing the high count rate limits of scintillation detectors for challenging neutron-capture experiments. *Nuclear Instruments and Methods in Physics Research A*, 1064:169385, July 2024.

75. N. Liu et al. Correlated Strontium and Barium Isotopic Compositions of Acid-cleaned Single Mainstream Silicon Carbides from Murchison. *ApJ*, 803(1):12, April 2015.
76. A. K. Speck et al. Silicon Carbide Absorption Features: Dust Formation in the Outflows of Extreme Carbon Stars. *ApJ*, 691(2):1202–1221, February 2009.
77. N. Liu. *Treatise on Geochemistry*, chapter Presolar Grains. Elsevier Inc., <https://doi.org/10.1016/B978-0-323-99762-1.00129-7>, 2025.
78. K. Takahashi and K. Yokoi. Beta-Decay Rates of Highly Ionized Heavy Atoms in Stellar Interiors. *Atomic Data and Nuclear Data Tables*, 36:375, January 1987.
79. D. Vescovi et al. Magnetic-buoyancy-induced Mixing in AGB Stars: Presolar SiC Grains. *ApJ*, 897(2):L25, July 2020.
80. M. Busso et al. s-processing in AGB Stars Revisited. III. Neutron Captures from MHD Mixing at Different Metallicities and Observational Constraints. *ApJ*, 908(1):55, February 2021.
81. S. Palmerini et al. Presolar Grain Isotopic Ratios as Constraints to Nuclear and Stellar Parameters of Asymptotic Giant Branch Star Nucleosynthesis. *ApJ*, 921(1):7, November 2021.
82. R. Mucciola et al. Evaluation of resonance parameters for neutron interactions with molybdenum. *Nuclear Instruments and Methods in Physics Research B*, 531:100–108, November 2022.
83. R. Mucciola et al. Neutron capture and total cross-section measurements on $^{94,95,96}\text{Mo}$ at n-TOF and GELINA. In *European Physical Journal Web of Conferences*, volume 284 of *European Physical Journal Web of Conferences*, pp. 01031, July 2023.
84. P. Bienvenu et al. A new determination of ^{79}Se half-life. *Applied Radiation and Isotopes*, 65(3):355–364, January 2007.
85. N. M. Chiera et al. Preparation of pbse targets for 79se neutron capture cross section studies. *Nuclear Instruments and Methods in Physics Research Section A: Accelerators, Spectrometers, Detectors and Associated Equipment*, 1029:166443, 2022.
86. N. M. Chiera et al. Preparation of PbSe targets for ^{79}Se neutron capture cross section studies. *Nuclear Instruments and Methods in Physics Research A*, 1029:166443, April 2022.
87. G. Walter et al. The s-process branching at Se-79. *The Astrophysical Journal*, 167(1):186–199, October 1986.
88. N. Klay and F. Käppeler. β -decay rate of ^{79m}Se and its consequences for the s-process temperature. *Phys. Rev. C*, 38(1):295–306, July 1988.
89. S. Amari et al. Presolar graphite from the Murchison meteorite: An isotopic study. *Geochimica et Cosmochimica Acta*, 133:479–522, May 2014.
90. S. Amari et al. Interstellar grains in meteorites: III. Graphite and its noble gases. *Geochim. Cosmochim. Acta*, 59(7):1411–1426, April 1995.
91. S. Amari et al. Large 18O Excesses in Circumstellar Graphite Grains from the Murchison Meteorite: Indication of a Massive-Star Origin. *ApJ*, 447:L147, July 1995.
92. G. Cescutti et al. Uncertainties in s-process nucleosynthesis in low-mass stars determined from Monte Carlo variations. *Monthly Notices of the Royal Astronomical Society*, 478(3):4101–4127, August 2018.
93. G. Cescutti et al. The s-Process Nucleosynthesis in Low Mass Stars: Impact of the Uncertainties in the Nuclear Physics Determined by Monte Carlo Variations. In *Nuclei in the Cosmos XV*, volume 219, pp. 297–300, August 2019.
94. N. Nishimura et al. Sensitivity to neutron captures and β -decays of the enhanced s-process in rotating massive stars at low metallicities. In *Journal of Physics Conference Series*, volume 940 of *Journal of Physics Conference Series*, pp. 012051, January 2018.
95. N. Nishimura et al. Impacts of nuclear-physics uncertainties in the s-process determined by Monte-Carlo variations. *arXiv e-prints*, pp. arXiv:1802.05836, February 2018.
96. C. Domingo-Pardo et al. Advances and new ideas for neutron-capture astrophysics experiments at CERN n-TOF. *European Physical Journal A*, 59(1):8, January 2023.
97. F. Käppeler. Reaction cross sections for the s, r, and p process. *Progress in Particle and Nuclear Physics*, 66(2):390–399, April 2011.
98. S. Bisterzo et al. s-Process in low-metallicity stars - I. Theoretical predictions. *MNRAS*, 404(3):1529–1544, May 2010.
99. S. Bisterzo and S. Cristallo. Low-metallicity AGB models: the H profile in the ^{13}C -pocket and the effect on the s-process. *Mem. Soc. Astron. Italiana*, 81:1095, January 2010.
100. F. Corvi et al. An experimental method for determining the total efficiency and the response function of a gamma-ray detector in the range 0.5–10 mev. *Nuclear Instruments and Methods in Physics Research Section A: Accelerators, Spectrometers, Detectors and Associated Equipment*, 265(3):475 – 484, 1988.
101. S. Amaducci et al. Measurement of the $^{140}\text{Ce}(n, \gamma)$ Cross Section at n-TOF and Its Astrophysical Implications for the Chemical Evolution of the Universe. *Phys. Rev. Lett.*, 132(12):122701, March 2024.
102. J. Balibrea-Correa et al. High precision $^{209}\text{Bi}(n, \gamma)$ cross section measurement at n-TOF EAR2. Technical report, CERN-INTC-2023-061 ; INTC-P-675; <https://cds.cern.ch/record/2872409>, 2023.
103. O. Straniero et al. s process in low-mass asymptotic giant branch stars. *Nucl. Phys. A*, 777:311–339, October 2006.
104. O. Straniero et al. Heavy Elements in Globular Clusters: The Role of Asymptotic Giant Branch Stars. *ApJ*, 785(1):77, April 2014.
105. R. N. Sahoo et al. Stellar s -process neutron capture cross section of Ce isotopes. *Phys. Rev. C*, 109(2):025808, February 2024.
106. J. J. Cowan and W. K. Rose. Production of ^{14}C and neutrons in red giants. *The Astrophysical Journal*, 212:149–158, February 1977.
107. P. A. Denissenkov et al. The impact of (n, γ) reaction rate uncertainties of unstable isotopes on the i-process nucleosynthesis of the elements from Ba to W. *MNRAS*, 503(3):3913–3925, May 2021.
108. C. Domingo-Pardo et al. Resonance capture cross section of Pb207. *Physical Review C*, 74(5):055802, November 2006.
109. C. Domingo-Pardo et al. Measurement of the neutron capture cross section of the s-only isotope Pb204 from 1 eV to 440 keV. *Physical Review C*, 75(1):015806, January 2007.

110. C. Domingo-Pardo et al. Measurement of the radiative neutron capture cross section of Pb206 and its astrophysical implications. *Physical Review C*, 76(4):045805, October 2007.
111. C. Massimi et al. n_TOF: Measurements of Key Reactions of Interest to AGB Stars. *Universe*, 8(2):100, February 2022.
112. C. Domingo Pardo et al. Neutron capture measurements on the s-process termination isotopes lead and bismuth. In A. Mengoni et al., editors, *International Symposium on Nuclear Astrophysics - Nuclei in the Cosmos*, pp. 58.1, January 2006.
113. S. Cristallo et al. Mass and metallicity distribution of parent AGB stars of presolar SiC. *A&A*, 644:A8, December 2020.
114. M. Lugaro et al. Do meteoritic silicon carbide grains originate from asymptotic giant branch stars of super-solar metallicity? *Geochim. Cosmochim. Acta*, 221:6–20, January 2018.
115. K. H. Guber et al. Neutron capture reaction rates for silicon and their impact on the origin of presolar mainstream SiC grains. *Phys. Rev. C*, 67(6):062802, June 2003.
116. C. Lederer-Woods et al. Measurement of $^{28,29,30}\text{Si}(n, \gamma)$ capture cross sections to explain isotopic abundances in presolar grains. Technical report, CERN-INTC-2023-009 ; INTC-P-653; <https://cds.cern.ch/record/2845928>, 2023.
117. G. Jörg et al. Preparation of radiochemically pure 79se and highly precise determination of its half-life. *Applied Radiation and Isotopes*, 68(12):2339–2351, 2010.
118. D. Schumann et al. How Radioactive Samples and Targets Can Help to Better Understand the Big Bang Theory. *Nuclear Physics News*, 26(4):20–25, October 2016.
119. H2020 Euratom.
120. HORIZON-EURATOM-2023-NRT-01.
121. D.Schumann, C. Stodel and M. Gott. 30th Conference of the International Nuclear Target Development Society (INTDS2022). In *Proceedings of the 30th Conferende of the International Nuclear Target Development Society*, 2023.
122. M. Lewitowicz (Chair), E. Widmann (Dep. Chair), G.E. Körner (Sci. Secr.). The NuPECC Long Range Plan for Nuclear Physics in Europe 2024. Technical report, EPS, 2024. www.nupecc.org/lrp2024/Documents/nupecc.lrp2024.pdf.
123. V. Babiano-Suárez et al. Imaging neutron capture cross sections: i-TED proof-of-concept and future prospects based on Machine-Learning techniques. *European Physical Journal A*, 57(6):197, June 2021.
124. E. Mendoza et al. Neutron capture measurements with high efficiency detectors and the Pulse Height Weighting Technique. *Nuclear Instruments and Methods in Physics Research A*, 1047:167894, February 2023.
125. M. E. Stamati et al. The n_TOF NEAR Station Commissioning and first physics case. In *European Physical Journal Web of Conferences*, volume 284 of *European Physical Journal Web of Conferences*, pp. 06009, July 2023.
126. G. Gervino et al. NEAR: A New Station to Study Neutron-Induced Reactions of Astrophysical Interest at CERN-n_TOF. *Universe*, 8(5):255, April 2022.
127. N. Patronis et al. The CERN n_TOF NEAR station for astrophysics- and application-related neutron activation measurements. *arXiv e-prints*, pp. arXiv:2209.04443, september 2022.
128. L. Zanini et al. Measurement of Volatile Radionuclides Production and Release Yields followed by a Post-Irradiation Analysis of a Pb/Bi Filled Ta Target at ISOLDE. *Nuclear Data Sheets*, 119:292–295, May 2014.
129. M. Turrión et al. Management of ISOLDE yields. *Nuclear Instruments and Methods in Physics Research B*, 266(19-20):4674–4677, October 2008.
130. J. Leredegui-Marco et al. Production of a ^{135}Cs sample at ISOLDE for (n, γ) activation measurements at n_TOF-NEAR. Technical report, CERN ISOLDE ; IS721; <https://cds.cern.ch/record/2834566>, 2022.
131. J. Leredegui-Marco et al. Activation measurements of the $^{135}\text{Cs}(n, \gamma)$ cross-section at n_TOF-NEAR. Technical report, CERN-INTC-2024-007 ; INTC-P-690; <https://cds.cern.ch/record/2886126>, 2024.
132. J. Leredegui-Marco et al. Measurement of the radiation background at the n_TOF NEAR facility to study the feasibility of cyclic activation experiments. Technical report, CERN-INTC-2022-018 ; INTC-I-241. <http://cds.cern.ch/record/2809131>, 2022.
133. C. Lederer-Woods et al. Neutron Activation Station at the SPS Beam Dump Facility (BDF). Technical report, CERN-SPSC-2024-027 ; SPSC-EOI-023; <https://cds.cern.ch/record/2913936>, 2024.
134. C. Ahdida et al. The SHiP experiment at the proposed CERN SPS Beam Dump Facility. *European Physical Journal C*, 82(5):486, May 2022.
135. R. Reifarth and Y. A. Litvinov. Measurements of neutron-induced reactions in inverse kinematics. *Physical Review Accelerators and Beams*, 17(1):014701, January 2014.
136. R. Reifarth et al. Spallation-based neutron target for direct studies of neutron-induced reactions in inverse kinematics. *Physical Review Accelerators and Beams*, 20(4):044701, April 2017.
137. A. L. Cooper et al. A high-intensity, low-energy heavy ion source for a neutron target proof-of-principle experiment at LANSCE. In *Journal of Physics Conference Series*, volume 2743 of *Journal of Physics Conference Series*, pp. 012091. IOP, May 2024.
138. R. Esposito et al. Design, testing, commissioning, and early operation of the third-generation n_TOF neutron spallation target at CERN. In *European Physical Journal Web of Conferences*, volume 285 of *European Physical Journal Web of Conferences*, pp. 07003, September 2023.
139. M. Grieser et al. Storage ring at HIE-ISOLDE. Technical design report. *European Physical Journal Special Topics*, 207(1):1–117, May 2012.
140. P. A. Butler et al. TSR: A storage and cooling ring for HIE-ISOLDE. *Nuclear Instruments and Methods in Physics Research B*, 376:270–274, June 2016.